

Thirty New Low-Mass Spectroscopic Binaries¹

Evgenya L. Shkolnik²

*Department of Terrestrial Magnetism, Carnegie Institution of Washington, 5241 Broad
Branch Road, NW, Washington, DC 20015*

shkolnik@dtm.ciw.edu

Leslie Hebb

*School of Physics and Astronomy, University of St. Andrews, North Haugh St Andrews,
Fife Scotland KY16 9SS, and Department of Physics and Astronomy, Vanderbilt
University, Nashville, TN 37235, USA*

leslie.hebb@vanderbilt.edu

Michael C. Liu³

*Institute for Astronomy, University of Hawaii at Manoa
2680 Woodlawn Drive, Honolulu, HI 96822*

mliu@ifa.hawaii.edu

I. Neill Reid

Space Telescope Science Institute, Baltimore, MD 21218

inr@stsci.edu

and

Andrew C. Cameron

*School of Physics and Astronomy, University of St. Andrews, North Haugh St Andrews,
Fife Scotland KY16 9SS*

Andrew.Cameron@st-and.ac.uk

ABSTRACT

As part of our search for young M dwarfs within 25 pc, we acquired high-resolution spectra of 185 low-mass stars compiled by the NStars project that have strong X-ray emission. By cross-correlating these spectra with radial velocity standard stars, we are sensitive to finding multi-lined spectroscopic binaries. We find a low-mass spectroscopic binary fraction of 16% consisting of 27 SB2s, 2 SB3s and 1 SB4, increasing the number of known low-mass SBs by 50% and proving that strong X-ray emission is an extremely efficient way to find M-dwarf SBs. WASP photometry of 23 of these systems revealed two low-mass EBs, bringing the count of known M dwarf EBs to 15. BD -22 5866, the SB4, is fully described in Shkolnik et al. (2008) and CCDM J04404+3127 B consists of a two mid-M stars orbiting each other every 2.048 days. WASP also provided rotation periods for 12 systems, and in the cases where the synchronization time scales are short, we used P_{rot} to determine the true orbital parameters. For those with no P_{rot} , we use differential radial velocities to set upper limits on orbital periods and semi-major axes. More than half of our sample has near-equal-mass components ($q > 0.8$). This is expected since our sample is biased towards tight orbits where saturated X-ray emission is due to tidal spin-up rather than stellar youth. Increasing the samples of M dwarf SBs and EBs is extremely valuable in setting constraints on current theories of stellar multiplicity and evolution scenarios for low-mass multiple systems.

Subject headings: binaries: spectroscopic, eclipsing; stars: late-type, activity, low-mass

¹Based on observations collected at the W. M. Keck Observatory, the Canada-France-Hawaii Telescope and by the WASP Consortium. The Keck Observatory is operated as a scientific partnership between the California Institute of Technology, the University of California, and NASA, and was made possible by the generous financial support of the W. M. Keck Foundation. The CFHT is operated by the National Research Council of Canada, the Centre National de la Recherche Scientifique of France, and the University of Hawaii. The WASP Consortium consists of astronomers primarily from the Queen’s University Belfast, St Andrews, Keele, Leicester, The Open University, Isaac Newton Group La Palma and Instituto de Astrofísica de Canarias. The SuperWASP Cameras were constructed and operated with funds made available from Consortium Universities and the UK’s Science and Technology Facilities Council.

²Carnegie Fellow

³Alfred P. Sloan Research Fellow

1. Introduction

The multiplicity of stars is an important constraint of star formation theories as most stars form as part of a binary or higher-order multiple system (e.g. Halbwachs et al. 2003; Bate 2009). Moreover, double- (or multi-) lined spectroscopic binaries (SBs) allow precise determination of dynamical properties including the mass ratio. The analysis of photometric and spectroscopic data of eclipsing binaries (EBs) provides radii, temperatures, luminosities and masses, arguably the most important stellar parameter, for two stars with same age and metallicity (Lastennet & Valls-Gabaud 2002) making them vital in calibrating stellar evolutionary models.

M dwarf EBs are particularly important since the radii of active M dwarfs are known to be 10-15% larger than existing models predict (López-Morales & Ribas 2005; Lopez-Morales et al. 2006; Torres et al. 2009). This discrepancy is thought to be caused by magnetic fields on active M dwarfs which inhibit convection (López-Morales 2007; Chabrier et al. 2007) and/or missing opacity sources in the models (Berger et al. 2006). Further study of the problem requires the identification and detailed study of more M dwarf EBs with a range of properties (e.g. masses, activity levels, metallicities, ages).

Though M dwarfs are ubiquitous in the Galaxy, composing 75% of known stars (Bochanski et al. 2008), their intrinsic faintness makes them difficult and costly to observe, and thus the multiplicity of M dwarfs has been a challenge to measure. A binary fraction of 57% has been well established for G dwarfs (Duquennoy & Mayor 1991), and there is clear consensus that the binary fraction of M dwarfs is significantly less than that. Published values range from 25% (Leinert et al. 1997) to 42% (Fischer & Marcy 1992) with the largest uncertainties likely due to incompleteness corrections. In addition to supplying key constraints for star formation theories, completing the M dwarf binary census of the solar neighborhood, which to date, is (near)-complete out to only 9 pc (Delfosse et al. 2004), is yet another goal in finding the nearby low-mass SBs.

Delfosse et al. (2004) presented what may be the most complete statistical study of M dwarfs, including both spectroscopic and visual binaries. They conclude a binary fraction of $26 \pm 3\%$ and that for M dwarfs, as for G dwarfs, the mass ratio ($q = M_B/M_A$) distribution is a function of orbital period with most shorter period binaries having near equal component masses, while wide binaries ($P_{orb} > 50$ days) have a flat q distribution. The different distribution in the two samples may point to two distinct formation mechanisms, one for long-period and one for short-period orbits.

Here we report on 30 low-mass SBs detected from 185 X-ray-selected M dwarfs in the solar neighborhood. Six of the targets were included in the Gliese catalog of which only one

was previously detected to be a SB. Prior to this work, 46 M dwarf SBs were published in the literature (Duquennoy & Mayor 1991; Delfosse et al. 1999; Fischer & Marcy 1992) with an additional 13 low-mass EBs (Shkolnik et al. 2008 and references therein and Blake et al. 2008). Thus our work increases the known sample of SBs by 50%.

We also searched the WASP photometric database in which we found 2 EBs and measured rotation periods of 12 binaries. Though rotation periods of single stars are important age indicators (e.g. Barnes 2007), for short-period binaries, where tidal locking is almost certain, the rotation periods offer true orbital periods instead.

2. Sample Selection

The original science goals of the X-ray-selected sample was to search for the youngest M dwarfs within 25 pc to identify the best possible stellar targets for direct imaging searches of extrasolar planets and circumstellar disks (Shkolnik et al. 2009). The Two Micron All Sky Survey (2MASS) is optimal for finding low-mass stars, since the SEDs of cool stars peak in the near-IR (e.g. Hawley et al. 2002). However, the *JHK* infrared passbands provide less distinctive spectral classification of early- and mid-M dwarfs (i.e. M2–M7 dwarfs have $(J-K)$ colors which span only 0.2 mag; Reid et al. 2007b) impeding the photometric distance determination. Thus, in order to fully characterize a volume-limited sample of young M dwarfs, a proper motion requirement of $\mu > 0.18'' \text{ yr}^{-1}$ was implemented, equivalent to a tangential velocity of 21 km s⁻¹ at 25 pc.

We drew ≈ 800 targets from the NStars 20-pc census (Reid et al. 2003, 2004) constructed from the 2MASS catalogs (Skrutskie et al. 2006) along with the Lépine et al. (2002) and Lépine & Shara (2005) proper motion catalogs, with an additional ~ 300 newly-catalogued M dwarfs that exhibit significant proper motion between the POSSI and 2MASS surveys (i.e. the Moving-M sample; Reid et al. 2007a). Distances were available either from parallaxes or spectrophotometric relations and are limited to 25 pc from the Sun, good to $\lesssim 15\%$ assuming all the stars were single and on the main-sequence (e.g., Reid & Cruz 2002; Cruz et al. 2003). Further details of the sample selection can be found in Shkolnik et al. (2009).

In order to characterize the youngest members of this sample, we acquired high-resolution spectra of the 185 cool dwarfs with bright X-ray luminosities. In Figure 1 we plot the fractional X-ray flux, F_X/F_J as a function of $I-J$, where F_X is the empirically calibrated *ROSAT* X-ray flux (Voges et al. 1999) using the count-rate conversion equation of Schmitt et al. (1995), and F_J is the 2MASS *J*-band flux. Target stars were chosen to have high X-ray emission ($\log(F_X/F_J) > -2.5$) near the saturation limit (Riaz et al. 2006) and comparable

to or greater than the fractional luminosities of Pleiades members (120 Myr, Micela et al. 1998) and β Pic members (12 Myr, Torres et al. 2006). We measured the radial velocities (RVs) needed to determine galactic space motion and young moving group membership (Shkolnik et al., in prep.). This process is also sensitive to finding SBs at any age, particularly those in short-period orbits where the tidal-locking forces rapid rotation producing high chromospheric and X-ray emission.

3. The spectra

We acquired spectra with the High Resolution Échelle Spectrometer (HIRES; Vogt et al. 1994) on the Keck I 10-m telescope and the Échelle SpectroPolarimetric Device for the Observation of Stars (ESPaDOnS; Donati et al. 2006) on the Canada-France-Hawaii 3.6-m telescope, both located on the summit of Mauna Kea.

We used the 0.861" slit with HIRES to give a spectral resolution of $\lambda/\Delta\lambda\approx 58,000$. The detector consists of a mosaic of three 2048 x 4096 15- μm pixel CCDs, corresponding to a blue, green and red chip spanning 4900 – 9200 Å. To maximize the throughput near the peak of a M dwarf spectral energy distribution, we used the GG475 filter with the red cross-disperser. The data product of each exposure is a multiple-extension FITS file from which we reduced and extracted the data from each chip separately.

ESPaDOnS is fiber fed from the Cassegrain to Coudé focus where the fiber image is projected onto a Bowen-Walraven slicer at the spectrograph entrance. With a 2048x4608-pixel CCD detector, ESPaDOnS' 'star+sky' mode records the full spectrum over 40 grating orders covering 3700 to 10400 Å at a spectral resolution of $\lambda/\Delta\lambda\approx 68,000$. The data were reduced using *Libre Esprit*, a fully automated reduction package provided for the instrument and described in detail by Donati et al. (1997, 2007).

All final spectra were of moderate S/N reaching ≈ 50 per pixel at 7000 Å. Each night, spectra were also taken of an A0V standard star for telluric line correction and an early-, mid- and late-M RV standard. To search for multi-lined binaries, we cross-correlated each of 7 orders between 7000 and 9000 Å of each stellar spectrum (from both instruments) with a RV standard of similar spectral type using IRAF's¹ *fxcor* routine (Fitzpatrick

¹IRAF (Image Reduction and Analysis Facility) is distributed by the National Optical Astronomy Observatories, which is operated by the Association of Universities for Research in Astronomy, Inc. (AURA) under cooperative agreement with the National Science Foundation.

1993).² We measure the RVs of each component from the gaussian peaks fitted to the cross-correlation function (CCF), taking the average of all orders, with a RMS typically less than 1 km s⁻¹ for both instruments. The resolved CCF peaks allowed us to estimate the spectral types, and thus component masses, of the individual stars assuming a flux-weighted relation between component and integrated spectral types (Daemgen et al. 2007): $\text{SpT}_{\text{int}} = (f_A \text{SpT}_A + f_B \text{SpT}_B) / (f_A + f_B)$. Evidence for this linear relationship is presented by Cruz & Reid (2002), which shows both the TiO and VO band depths vary linearly with SpT for stars ranging from M0 to M7. SpT_{int} was measured from the ratio of the band indices of TiO $\lambda 7140$ to TiO $\lambda 8465$ defined by Slesnick et al. (2006) and calibrated with 136 M dwarfs of known SpT (Shkolnik et al. 2009). f_A and f_B were derived from the integrated “flux” of the gaussian fits to the cross-correlation peaks. An additional restriction to the spectral types of the two components is provided by ΔR , where $\Delta R = M_R(\text{SpT}_B) - M_R(\text{SpT}_A)$. These two equations together produce a unique solution for the component spectral types, which are good to 0.5 subclasses or better. The integrated properties of the binary systems, including the systemic velocity γ and the corrected photometric distance, are listed in Table 1 with a histogram of the component SpTs in Figure 2. We can estimate the mass of the components from these SpTs using the mass relationship from Reid & Hawley (2005), which is based on the 8-pc sample of M dwarfs originally presented in Reid & Gizis (1997). The error on the masses ranges from 10% for M0 to 40% for M6, mostly due to the error in spectral typing the two components.

4. WASP Photometry

We cross-correlated our sample of M dwarf SBs with the UK Wide-Angle Search for Planets (WASP) database (Pollacco et al. 2006) and identified 23 observed systems, of which 12 have clear rotational modulation, including 2 new EBs.

WASP is a wide-field photometric variability survey of bright stars designed to detect significant numbers of transiting gas giant planets. The survey operates two robotic telescopes, one in each hemisphere, which repeatedly observe nearly the entire visible sky every clear night. The resulting data product of the ongoing survey consists of high cadence (~ 8 minute sampling), precise ($\sim 1\%$ r.m.s.), single-band light curves for millions of bright ($V = 9 - 13$) stars with spectral types that cover the Hertzsprung-Russell diagram. Each stellar light curve typically has several thousand photometric data points obtained over several years with typical photometric precision of 0.007 – 7 mag per observing season for the

²See Table 3 of Shkolnik et al. (2009) for the list of RV standards used.

above magnitude range. The stars that are observed exist in all regions of the sky except the Galactic plane due to crowding and extinction and the equatorial poles, which have yet to be surveyed. The WASP survey is the most successful transiting planet survey to date and has discovered over 20 new transiting gas giant planets (e.g. Cameron et al. 2007; Anderson et al. 2008; West et al. 2009; Hebb et al. 2009; Hellier et al. 2009). However, for our SB targets, we are able to detect rotational variability with an amplitude $\lesssim 0.01$ mags.

4.1. Rotation Periods

Asymmetrically distributed starspots on the photosphere of one or more components of the binary will cause periodic brightness variations as the spots rotate in and out of view with the star. The stellar rotation period (or a harmonic) can be identified through the detection of a periodic sinusoidal variability signal. Starspots typically evolve on timescales of weeks to months which leads to changes in the amplitude and/or phase of the variability, thus we independently searched each season of photometric WASP data to maximize our chances of detecting a periodic signal.

To measure the level of periodic variability in each target, we determined the improvement in χ^2 over a flat, non-variable model ($\delta\chi^2$) when a sine wave of the form $y = a_0 + a_1\sin(\omega t + a_3)$ was fit to each season of the WASP data phase-folded at a set of trial periods, $P_{rot} = 2\pi/\omega$. Periods between 0.2–30 days were searched. The statistic, $\delta\chi^2/\chi_{best}^2$ (Zechmeister & Kürster 2009), where χ_{best}^2 is the χ^2 with respect to the best fitting sinusoidal model, was used to distinguish genuine variability in each light curve. Our sensitivity to the period detection is different for each object, but in general, we can detect a sinusoidal signal with an amplitude of > 5 mmag and a period, $P_{rot} < 30$ days.

Twelve of the 23 M dwarf SBs with WASP data³ show periodic sinusoidal variability in at least one season of WASP data. These are listed in Table 3 and their phase-folded light curves are shown in Figure 4. We note that four of the systems have multiple seasons of data in which the same or a similar period is detected which provides additional confirmation of the period detection. No variability is seen in the remaining 11 targets for which we have time-series data (Table 4). In both tables, we first list the target and the number of data points available in each season as well as the HJD of the starting and ending dates for the light curve. We also list the value of the $\delta\chi^2/\chi_{best}^2$ statistic for the highest peak in the periodogram. All the positive detections have $\delta\chi^2/\chi_{best}^2 \geq 0.29$ and the non-detections typically have $\delta\chi^2/\chi_{best}^2 < 0.15$. For the positive detections, we also list the rotation period

³Seven of the SBs have not yet been sufficiently observed by WASP or are not accessible to the telescopes.

and the amplitude of the variability.

4.2. Low-mass eclipsing binaries

In addition to discovering transiting extrasolar planets, the time-series photometry obtained through the WASP survey is an excellent data set for identifying eclipsing binary stars. Therefore, we searched the WASP light curves of the SB sample for periodic eclipses. We employed the WASP implementation of the box-least squares (BLS) algorithm (Kovács et al. 2002; Collier Cameron et al. 2006) which is designed to detect square-shaped dips in brightness in an otherwise flat light curve. The BLS algorithm is efficient at detecting both transiting planets (Tingley 2003) and EBs (Hartman et al. 2009). We searched periods between 0.5-10 days and detected two eclipsing binaries. BD -22 5866 is a late-type quadruple system composed of two binary pairs (K7+K7 and M1+M2) in which the more massive binary is eclipsing with a 2.21 day period. This unique system is described in Shkolnik et al. (2008).

The second EB we detected in the M dwarf SB sample is CCDM J04404+3127 B. The object is part of a triple system composed of the EB with a proper motion companion $\sim 15''$ away (CCDM J04404+3127 A). The photometry shows an eclipsing light curve for CCDM J04404+3127 (Figure 3), but since the A and B components of the multiple system are blended in the large photometric aperture ($\sim 48''$), the WASP data alone cannot determine which component is the unresolved EB.⁴ However, given that CCDM J04404+3127 A does not have a ROSAT detection and the single spectrum of CCDM J04404+3127 B presented here confirms it be a spectroscopic binary, it must also be the EB.

The target was observed by the SuperWASP camera on La Palma, Canary Islands in the 2004 and 2006 observing seasons. The existing photometric data consists of 949 measurements taken between 1 August and 29 September 2004 and 2478 measurements taken from 29 September 2006 to 15 February 2007. After detecting the eclipsing binary using the BLS algorithm described above, we fit a more realistic eclipsing light curve model to the combined light curve to derive an accurate ephemeris for the system. We used the JKT Eclipsing Binary Orbit Program (EBOP; Popper & Etzel 1981; Southworth et al. 2007) to derive an ephemeris of:⁵

$$\text{Min(HJD)} = (2454129.2969 \pm 0.0007) + (2.048135 \pm 0.000003)E$$

⁴Hartman et al. (2009) also identify this object (HAT-216-0003316) as a probable EB based on HAT transiting planet survey data, but the object is blended with CCDM J04404+3127 A in their data as well.

⁵The ephemeris reported here is consistent with the period determined by Hartman et al. (2009).

Due to the contamination by light from CCDM J04404+3127 A, we cannot confidently report any other parameters for the system until more data is collected. However from the spectrum, the EB consists of a M4.2 and a M5.0 dwarf.

5. Binary Properties

5.1. Tidal Synchronization and Maximal Orbits

With a single spectroscopic observation, the difference between the radial velocity of each component (ΔRV) provides an upper limit to the orbital period and semi-major axis using the stellar masses determined from the integrated fluxes (i.e. the area) of the cross-correlation peaks. However, the added photometry of WASP can provide a true orbital period and semi-major axis if the stellar system is expected to be tidally synchronized, i.e. $P_{orb} = P_{rot}$.

The tidal synchronization time scale t_{sync} of close-in binary systems is fairly short, e.g. less than 200 Myr for two 0.5- M_{\odot} stars with $P_{orb}=5$ days as calculated using Equation 6.1 of Zahn (1977). Drake et al. (1998) show that Zahn’s values serve as an upper limit to the time needed to synchronize the upper envelopes of the stars and thus the time that it would take for P_{rot} to equal P_{orb} may be > 3 times shorter than t_{sync} . Such time scales are comparable to the lithium depletion time scale, which ranges from 15 Myr for a M0 to 90 Myr for a M6 dwarf (Chabrier et al. 1996). We do not detect any lithium in these stars, nor any other spectroscopic indication that the stars are young (e.g. low surface gravity and strong $H\alpha$ emission), and thus the stars are almost certainly older than > 0.2 Gyr.

Of the 12 binaries with measured rotation periods, 2 have calculated t_{sync} (using a_{max}) of less than 200 Myr. For these systems, we assume that the binaries are synchronized such that the observed photometric period is equal to both the rotation *and* orbital periods. These periods and corresponding semi-major axes are listed in Table 2. For those stars where there is no photometric data or the photometric period is long enough such that if it were the orbital period $t_{sync} \gg 10$ Gyr, we list the maximal orbital parameters, P_{max} and a_{max} .

With only one ΔRV measurement, we cannot assume tidal synchronicity in those systems with short rotational periods but with long t_{sync} . The rapid rotation of one or both of the components may be due to a young system in a wider orbit. Although we can set some lower limits on the ages of the stars using surface gravity indices and the lack of lithium absorption, these limits are generally short compared to the spin-down rate of M dwarfs. Delfosse et al. (1998) reported that early M’s spin down to 2 km s^{-1} or less (or $P_{rot} = 10 - 15$ days) by 500 Myr while late Ms take ~ 1 Gyr to spin down to 2 km s^{-1} . These time

scales are comparable to the statistical investigations of West et al. (2008). And, given that the sample was selected for strong X-ray luminosity, we cannot rule out that our SB sample maybe indeed contain young M dwarfs in wide binary systems. However, it remains probable that all the stars in this sample will eventually be shown to be close-in, rapidly orbiting and rotating SBs.

5.2. X-ray saturation in short-period systems

At least 12 of the 30 systems have orbital periods less than 4.5 days (Figure 5) clearly displaying our bias towards tidally spun-up stars. Data compiled by Riaz et al. (2006) of a large set of M dwarfs suggest that the coronal activity remains at a high level independent of SpT and age implying that rotation, not age, dominates the magnetic activity in low-mass stars.

Recently, Reiners et al. (2009) measured that in M dwarfs the surface magnetic flux also saturates, similar to the activity implying that a star with saturated levels of X-ray emission does not necessarily have a large filling factor (i.e. the whole star need not be covered with active regions). This is supported by the clear rotation periods we detect. However, there are three targets, all of which are mid-Ms, (2MASS J0808+4347, HAT 199-13890, and LSPM J2114+1254) for which there is no modulated photometric signal and yet the maximum orbital periods are quite short (< 3 days). In these cases, we suspect that the filling factor is indeed high, such that the symmetric spots do not produce any photometric variability. This is supported by spectropolarimetric observation by Morin et al. (2008) who report that a sample of 5 mid-M stars mainly host axisymmetric large-scale poloidal fields.

5.3. Mass Ratios

Past studies of SBs have somewhat crudely shown that the mass ratio q , is inversely correlated with the mass of the primary star. For solar-type stars, q peaks at about 0.2 (Duquennoy & Mayor 1991), while Halbwachs et al. (2003) found a bimodal distribution for A to K type stars: q has a broad distribution between 0.2 and 0.7 for long orbital periods, and a strong peak with near equal-mass systems, primarily in shorter orbital period (< 100 days). For M dwarfs, Fischer & Marcy (1992) measured a flat distribution for q over all periods in a sample of visual and spectroscopic binaries. Although our range for q matches theirs (0.4 – 1; Figure 6), more than half of our sample has $q > 0.8$, which is not the case in the Fischer & Marcy (1992) sample. This is expected since our sample is biased towards

tight orbits where the primary selection criterion of saturated X-ray emission is due to tidal spin-up. In addition, these binaries with large q will synchronize much more quickly as $t_{sync} \propto q^{-2}$.

6. Conclusions

Of our sample of 185 X-ray bright M dwarfs, we find a low-mass, multi-lined spectroscopic binary fraction of 16%. These 30 SBs are composed of 27 SB2s, 2 SB3s and 1 SB4, increasing the number of known low-mass SBs by 50% and proving that strong X-ray emission is an extremely efficient way to find M-dwarf SBs.

To search for single-lined SBs (SB1), we observed two epochs (separated typically by 2–3 months) of 65 of the 185 targets, none of which showed a significant RV variation between visits to the level of 1 km s^{-1} . This implies that the single-lined binary fraction of stars with orbital periods of less than about 1.5 years in our sample is very low, less than 1.5%, and that M dwarf binaries with low mass ratios ($q \ll 1$) are rare. It is possible that up to 4%⁶ of the stars with a single observation are indeed double-lined SBs if the systems were in conjunction at the times of the observation. Combining this with the $\leq 1.5\%$ chance of observing an SB1, there are at most a handful of undiscovered SBs in the original 185 ROSAT-selected targets, setting an upper limit of 19% to the SB fraction (with $P_{orb} \lesssim 1.5$ years) of our sample.

WASP photometry of 23 of these systems revealed two low-mass EBs, bringing the count of known M dwarf EBs to 15. The WASP data also provided rotation periods for 12 systems, and in the cases where the synchronization time scales are short, orbital periods and semi-major axes.

This X-ray bright sample of 30 SBs is strongly biased towards high- q , tidally-synchronized binaries. In addition to being in short-period orbits, they are also relatively bright, making them excellent targets for a spectroscopic monitoring program to measure the component velocities necessary to determine the Keplerian orbital parameters for more precise mass ratios, and in the case of the eclipsing systems, the individual masses needed to test evolutionary models.

⁶This 4% limit is based on the time a close-in low-mass binary with an orbital period of 5 days would spend near conjunction such that the RVs of the two components would not produce resolved peaks in the CCF.

We thank the anonymous referee for her/his insightful comments on the original manuscript. E.S also thanks the CFHT and Keck staff for their care in setting up the instruments and support in the control room. This material is based upon work supported by the Carnegie Institution of Washington and the National Aeronautics and Space Administration through the NASA Astrobiology Institute and the NASA/GALEX grant program under Cooperative Agreement Nos. NNA04CC08A and NNX07AJ43G issued through the Office of Space Science. M.C.L. acknowledges support from the Alfred P. Sloan Research Fellowship.

REFERENCES

- Anderson, D. R., et al. 2008, MNRAS, 387, L4
- Barnes, S. A. 2007, ApJ, 669, 1167
- Bate, M. R. 2009, MNRAS, 392, 590
- Berger, D. H., et al. 2006, ApJ, 644, 475
- Blake, C. H., Torres, G., Bloom, J. S., & Gaudi, B. S. 2008, ApJ, 684, 635
- Bochanski, J. J., Hawley, S. L., Reid, I. N., Covey, K. R., West, A. A., Golimowski, D. A., & Ivezić, Z. 2008, ArXiv e-prints
- Cameron, A. C., et al. 2007, MNRAS, 375, 951
- Chabrier, G., Baraffe, I., & Plez, B. 1996, ApJ, 459, L91+
- Chabrier, G., Gallardo, J., & Baraffe, I. 2007, A&A, 472, L17
- Collier Cameron, A., et al. 2006, MNRAS, 373, 799
- Cruz, K. L., & Reid, I. N. 2002, AJ, 123, 2828
- Cruz, K. L., Reid, I. N., Liebert, J., Kirkpatrick, J. D., & Lowrance, P. J. 2003, AJ, 126, 2421
- Daemgen, S., Siegler, N., Reid, I. N., & Close, L. M. 2007, ApJ, 654, 558
- Delfosse, X., et al. 2004, in *Astronomical Society of the Pacific Conference Series*, Vol. 318, *Spectroscopically and Spatially Resolving the Components of the Close Binary Stars*, ed. R. W. Hilditch, H. Hensberge, & K. Pavlovski, 166–174
- Delfosse, X., Forveille, T., Beuzit, J.-L., Udry, S., Mayor, M., & Perrier, C. 1999, A&A, 344, 897
- Delfosse, X., Forveille, T., Perrier, C., & Mayor, M. 1998, A&A, 331, 581
- Drake, S. A., Pravdo, S. H., Angelini, L., & Stern, R. A. 1998, AJ, 115, 2122
- Duquennoy, A., & Mayor, M. 1991, A&A, 248, 485
- Fischer, D. A., & Marcy, G. W. 1992, ApJ, 396, 178
- Halbwachs, J. L., Mayor, M., Udry, S., & Arenou, F. 2003, A&A, 397, 159

- Hartman, J. D., Bakos, G. Á., Noyes, R. W., Sipöcz, B., Kovács, G., Mazeh, T., Shporer, A., & Pál, A. 2009, ArXiv e-prints
- Hawley, S. L., et al. 2002, *AJ*, 123, 3409
- Hebb, L., et al. 2009, *ApJ*, 693, 1920
- Hellier, C., et al. 2009, *Nature*, 460, 1098
- Hünsch, M., Schmitt, J. H. M. M., Sterzik, M. F., & Voges, W. 1999, *A&AS*, 135, 319
- Kovács, G., Zucker, S., & Mazeh, T. 2002, *A&A*, 391, 369
- Lastennet, E., & Valls-Gabaud, D. 2002, *A&A*, 396, 551
- Leinert, C., Henry, T., Glindemann, A., & McCarthy, Jr., D. W. 1997, *A&A*, 325, 159
- Lépine, S., & Shara, M. M. 2005, *AJ*, 129, 1483
- Lépine, S., Shara, M. M., & Rich, R. M. 2002, *AJ*, 124, 1190
- López-Morales, M. 2007, *ApJ*, 660, 732
- Lopez-Morales, M., Orosz, J. A., Shaw, J. S., Havelka, L., Arevalo, M. J., McIntyre, T., & Lazaro, C. 2006, ArXiv Astrophysics e-prints
- López-Morales, M., & Ribas, I. 2005, *ApJ*, 631, 1120
- Micela, G., Sciortino, S., Harnden, Jr., F. R., & Rosner, R. 1998, *Ap&SS*, 261, 105
- Morin, J., et al. 2008, *MNRAS*, 390, 567
- Perryman, M. A. C., & ESA, eds. 1997, ESA Special Publication, Vol. 1200, The HIPPARCOS and TYCHO catalogues. Astrometric and photometric star catalogues derived from the ESA HIPPARCOS Space Astrometry Mission
- Pollacco, D. L., et al. 2006, *PASP*, 118, 1407
- Popper, D. M., & Etzel, P. B. 1981, *AJ*, 86, 102
- Reid, I. N., & Cruz, K. L. 2002, *AJ*, 123, 2806
- Reid, I. N., et al. 2003, *AJ*, 126, 3007
- . 2004, *AJ*, 128, 463

- Reid, I. N., Cruz, K. L., & Allen, P. R. 2007a, *AJ*, 133, 2825
- Reid, I. N., & Gizis, J. E. 1997, *AJ*, 113, 2246
- Reid, I. N., & Hawley, S. L. 2005, *New light on dark stars : red dwarfs, low-mass stars, brown dwarfs*, ed. I. N. Reid & S. L. Hawley
- Reid, I. N., Kirkpatrick, J. D., Liebert, J., Gizis, J. E., Dahn, C. C., & Monet, D. G. 2002, *AJ*, 124, 519
- Reid, I. N., Turner, E. L., Turnbull, M. C., Mountain, M., & Valenti, J. A. 2007b, *ApJ*, 665, 767
- Reiners, A., Basri, G., & Browning, M. 2009, *ApJ*, 692, 538
- Riaz, B., Gizis, J. E., & Harvin, J. 2006, *AJ*, 132, 866
- Schmitt, J. H. M. M., Fleming, T. A., & Giampapa, M. S. 1995, *ApJ*, 450, 392
- Shkolnik, E., Liu, M. C., & Reid, I. N. 2009, *ApJ*, 699, 649
- Shkolnik, E., Liu, M. C., Reid, I. N., Hebb, L., Cameron, A. C., Torres, C. A., & Wilson, D. M. 2008, *ApJ*, 682, 1248
- Skrutskie, M. F., et al. 2006, *AJ*, 131, 1163
- Slesnick, C. L., Carpenter, J. M., & Hillenbrand, L. A. 2006, *AJ*, 131, 3016
- Southworth, J., Bruntt, H., & Buzasi, D. L. 2007, *A&A*, 467, 1215
- Tingley, B. 2003, *A&A*, 408, L5
- Torres, C. A. O., Quast, G. R., da Silva, L., de La Reza, R., Melo, C. H. F., & Sterzik, M. 2006, *A&A*, 460, 695
- Torres, G., Andersen, J., & Gimenez, A. 2009, *ArXiv e-prints*
- Voges, W., et al. 1999, *A&A*, 349, 389
- West, A. A., Hawley, S. L., Bochanski, J. J., Covey, K. R., Reid, I. N., Dhital, S., Hilton, E. J., & Masuda, M. 2008, *AJ*, 135, 785
- West, R. G., et al. 2009, *AJ*, 137, 4834
- Worley, C. E., & Douglass, G. G. 1997, *A&AS*, 125, 523

Zahn, J.-P. 1977, A&A, 57, 383

Zechmeister, M., & Kürster, M. 2009, A&A, 496, 577

Table 1. M dwarf Spectroscopic Binaries

Name	RA & DEC J2000	SpT _{int} M-(±0.5)	<i>I</i> <i>USNO</i>	<i>J</i> <i>2MASS</i>	log(<i>F_X</i> / <i>F_J</i>) ^a	γ km s ⁻¹	HJD -2450000	Dist. ^b pc	Binarity ^c
2MASS J00080642+4757025	00 08 06.4 +47 57 02.0	3.6	10.1	8.523	-2.387	-29.64 ± 0.44	3961.10494	16.2 ± 1.9	SB2
LHS 6032	01 45 18.2 +46 32 07.8	1.7	9.94	8.058	-2.130	17.85 ± 0.69	4288.12715	26.7 ± 2.7	SB2, VB (NE)
G 274-113	01 53 11.3 -21 05 43.0	1.3	10.04	8.066	-2.384	14.48 ± 0.51	4378.96250	28.6 ± 2.0	SB2
NLTT 6638	01 59 12.6 +03 31 11.3	2.5	–	7.998	-2.413	-9.48 ± 0.74	4288.13890	11.2 ± 2.7	SB2, VB (NE)
GJ 3129	02 02 44.2 +13 34 33.0	4.7	10.9	9.652	-2.225	-12.94 ± 0.60	4378.98460	22.7 ± 2.2	SB2
GJ 3236	03 37 14.1 +69 10 49.8	4.1	10.91	9.806	-2.279	16.95 ± 3.55	4155.81744	22.0 ± 2.7	SB2
NLTT 11415	03 37 33.4 +17 51 14.5	1.9	9.85	9.1	-2.291	40.22 ± 0.51	4155.82919	31.3 ± 2.7	SB2, VB of GJ3240B
GJ 3240 B	03 37 33.9 +17 51 00.4	4.3	10.19	9.186	-2.256	38.25 ± 3.57	3725.98033	21.9 ± 2.7	E?SB2, VB
2MASS J04244260-0647313	04 24 42.6 -06 47 31.0	5.2	10.93	9.566	-2.066	13.05 ± 0.77	3726.00509	17.9 ± 1.6	SB3
CCDM J04404+3127B	04 40 23.0 +31 26 46.2	4.5	11.22	10.023	-2.359	41.73 ± 1.19	3726.03777	30.5 ± 2.7	ESB2, VB
GJ 206	05 32 14.7 +09 49 15.0	4.1	9.7	7.423	-2.391	20.66 ± 0.63	3726.08132	12.8 ± 0.6 ^d	SB2
GJ 3362	05 40 16.1 +12 39 00.8	1.4	10.38	8.072	-2.400	95.12 ± 1.68	3726.08645	22.4 ± 2.7	SB2
G 108-4	06 29 50.2 -02 47 45.0	5.7	10.76	9.468	-2.266	83.59 ± 0.38	3726.11372	37.6 ± 2.2	SB2
2MASS J07282116+3345127	07 28 21.2 +33 45 12.0	3.9	10.45	9.28	-2.444	11.34 ± 1.04	3866.72743	32.7 ± 3.7	SB2
LHS 5134	08 08 13.6 +21 06 09.0	2.6	–	7.336	-2.327	82.87 ± 0.75	3726.12839	17.1 ± 0.8 ^d	SB2, VB
2MASS J08082487+4347557	08 08 24.9 +43 47 55.0	5.5	12.56	10.493	-2.267	72.95 ± 0.57	3726.12411	22.4 ± 2.6	SB2
GJ 1108 B	08 08 55.4 +32 49 04.7	3.0	–	7.999	-2.053	12.12 ± 0.70	3866.77237	20.7 ± 1.5 ^d	SB2, VB
GJ 3547	09 19 22.9 +62 03 16.8	0.0	9.99	8.168	-2.530	68.52 ± 1.21	3866.82837	32.5 ± 2.8 ^d	SB2
GJ 3630	10 52 03.3 +00 32 38.3	4.8	10.71	9.426	-2.040	25.88 ± 1.35	3726.14401	19.0 ± 2.7	SB3
2MASS J12065663+7007514	12 06 56.6 +70 07 51.4	3.9	9.1	9.251	-2.296	-21.81 ± 0.53	4455.04585	16.8 ± 1.9	SB2, VB (W)
2MASS J14204953+6049348	14 20 49.5 +60 49 34.0	3.5	11.16	10.06	-2.473	-23.15 ± 0.85	3960.75723	44.6 ± 5.1	SB2
GJ 616.2	16 17 05.4 +55 16 09.0	1.2	8.55	6.6	-2.487	-28.25 ± 0.92	3960.79603	20.7 ± 0.5 ^d	SB2, VB
HAT 199-13890	19 31 12.6 +36 07 30.0	5.1	10.88	9.609	-2.020	-22.31 ± 1.24	3867.04116	21.7 ± 1.8	SB2, VB
NLTT 48838	20 10 34.5 +06 32 14.1	3.6	9.6	8.021	-2.186	-52.15 ± 1.25	3960.87589	15.3 ± 2.7	SB2
2MASS J21021569-3129118	21 02 15.6 -31 29 11.0	4.3	11.26	9.853	-2.384	-6.98 ± 0.42	3867.12034	16.9 ± 2.2	SB2
LSPM J2114+1254	21 14 49.1 +12 54 00.2	5.5	11.21	9.908	-2.358	-58.58 ± 0.50	3867.11455	27.8 ± 2.7	SB2
BD -225866	22 14 38.4 -21 41 53.0	0.0	9.21	7.54	-2.713	-14.07 ± 2.43	3867.12294	40.1 ± 3.2	ESB4
G 67-46	23 06 23.8 +12 36 26.7	0.7	10.45	8.375	-2.356	-3.53 ± 0.96	3960.96632	34.3 ± 2.7	SB2(3?), VB
GJ 4359	23 43 59.5 +64 44 28.9	0.8	10.1	8.149	-2.386	14.56 ± 1.08	3960.98538	28.9 ± 1.7 ^d	SB2
GJ 4362	23 48 36.0 -27 39 38.0	2.1	9.86	8.584	-2.448	25.30 ± 0.55	3961.08236	24.6 ± 1.9	SB2

^aJ band fluxes calculated here use the full 2MASS bandwidth of 0.29 μm .^bPhotometric distances from Reid et al. (2002, 2007a) were corrected for the over-luminosity of the binary system.

^cThose targets with directions in parentheses were resolved as visual binaries (VB) at the telescope. Those without directions, are listed as VBs in the Washington Visual Double Star Catalog (Worley & Douglass 1997). Eclipsing SBs are designated as “ESB?”.

^dDistances using trigonometric parallaxes from the Hipparcos & Tycho Catalogues (Perryman & ESA 1997).

Table 2. RVs & Orbital Parameters

Name	SpT M-(± 0.5)	Mass ^a M_{\odot}	q	RV km s^{-1}	P_{rot}^b days	P_{orb} days	a AU	t_{sync} Gyr
2MASS J00080642+4757025 A	3.6	0.2	1.00	17.01 ± 0.33	4.38	4.4 ^c	0.04	0.151
2MASS J00080642+4757025 B	3.5	0.2		-76.30 ± 0.29				
LHS 6032 A	1.9	0.44	1.00	36.56 ± 0.53	4.05	<157.9	<0.56	$\gg 10$
LHS 6032 B	1.6	0.44		-0.86 ± 0.45				
G 274-113 A	1.1	0.49	1.00	-53.72 ± 0.25	2.90	2.9 ^c	0.04	0.027
G 274-113 B	1.4	0.49		82.68 ± 0.44				
NLTT 6638 A	2.2	0.44	0.82	-23.29 ± 0.67	31.10	< 356.4	<0.93	$\gg 10$
NLTT 6638 B	3.0	0.36		4.34 ± 0.31				
GJ 3129 A	4.4	0.2	0.70	-37.25 ± 0.47	4.00	<27.8	<0.13	$\gg 10$
GJ 3129 B	5.2	0.14		11.36 ± 0.38				
GJ 3236 A	3.8	0.2	1.00	45.39 ± 2.90	no data	<20.4	<0.11	$\gg 10$
GJ 3236 B	4.4	0.2		-11.49 ± 2.05				
NLTT 11415 A	1.5	0.49	0.41	11.20 ± 0.17	not variable	<33.2	<0.18	$\gg 10$
NLTT 11415 B	3.6	0.2		69.25 ± 0.48				
GJ 3240 Ba	4.2	0.2	1.00	-66.23 ± 2.81	not variable	<0.4	0.01	1.E-05
GJ 3240 Bb	4.3	0.2		142.72 ± 2.20				
2MASS J04244260-0647313 A	4.5	0.17	0.77	-11.86 ± 0.38	no data	<70.3	<0.25	$\gg 10$
2MASS J04244260-0647313 Ba	5.5	0.12	0.83	77.03 ± 0.78		<1.9	<0.02	0.011
2MASS J04244260-0647313 Bb	5.7	0.1		-26.03 ± 0.67				
CCDM J04404+3127 Ba	4.2	0.2	0.70	-7.78 ± 0.64	2.048 (EB)	2.0	0.02	0.011
CCDM J04404+3127 Bb	5.0	0.14		91.24 ± 1.00				
GJ 206 A	3.9	0.2	1.00	0.93 ± 0.34	7.60	<61.1	<0.23	1.4
GJ 206 B	4.3	0.2		40.40 ± 0.52				
GJ 3362 A	1.1	0.49	0.90	75.23 ± 1.43	no data	<138.9	<0.52	$\gg 10$
GJ 3362 B	2.0	0.44		115.01 ± 0.88				
G 108-4 A	5.0	0.14	0.71	101.78 ± 0.28	no data	<46.9	<0.16	$\gg 10$
G 108-4 B	6.3	0.1		65.41 ± 0.26				
2MASS J07282116+3345127 A	3.9	0.2	1.00	-1.30 ± 0.79	3.55	<232.7	<0.55	$\gg 10$
2MASS J07282116+3345127 B	3.9	0.2		23.98 ± 0.67				
LHS 5134 A	2.4	0.44	0.82	66.52 ± 0.31	9.70	<215.0	<0.66	6.5
LHS 5134 B	3.1	0.36		99.23 ± 0.69				

Table 2—Continued

Name	SpT M-(±0.5)	Mass ^a M_{\odot}	q	RV km s ⁻¹	P_{rot}^b days	P_{orb} days	a AU	t_{sync} Gyr
2MASS J08082487+4347557 A	5.1	0.14	0.71	16.21 ± 0.48	not variable	<1.5	<0.02	0.062
2MASS J08082487+4347557 B	6.1	0.1		129.70 ± 0.30				
GJ 1108 Ba	2.8	0.36	1.00	-1.06 ± 0.53	3.38	<395.5	<0.92	≫10
GJ 1108 Bb	3.3	0.36		25.30 ± 0.45				
GJ 3547 A	-0.1	0.6	1.00	27.36 ± 0.93	no data	<20.2	<0.16	≫10
GJ 3547 B	0.1	0.6		109.68 ± 0.77				
GJ 3630 A	4.3	0.2	0.91	26.14 ± 1.27	not variable	<6E7	<2313	≫10
GJ 3630 Ba	5.5	0.12	0.83	-16.58 ± 0.45		<28.1	<0.11	≫10
GJ 3630 Bb	6.1	0.1		68.06 ± 0.65				
2MASS J12065663+7007514 A	3.9	0.2	1.00	34.13 ± 0.38	no data	<2.7	<0.03	0.024
2MASS J12065663+7007514 B	3.9	0.2		-77.75 ± 0.37				
2MASS J14204953+6049348 A	3.2	0.36	0.56	-33.76 ± 0.75	no data	0.4	0.01	3E-5
2MASS J14204953+6049348 B	3.8	0.2		-12.54 ± 0.39				
GJ 616.2 A	1.1	0.49	1.00	-41.20 ± 0.75	not variable	<530.6	<1.30	≫10
GJ 616.2 B	1.4	0.49		-15.31 ± 0.54				
HAT 199-13890 A	5.0	0.14	1.00	-100.14 ± 0.79	not variable	<0.7	<0.01	0.002
HAT 199-13890 B	5.1	0.14		55.53 ± 0.96				
NLTT 48838 A	3.5	0.36	0.56	-77.56 ± 0.67	1.12	<40.1	<0.19	≫10
NLTT 48838 B	3.8	0.2		-26.75 ± 1.05				
2MASS J21021569-3129118 A	4.4	0.2	1.00	-32.70 ± 0.30	not variable	<27.6	<0.13	≫10
2MASS J21021569-3129118 B	4.2	0.2		18.74 ± 0.30				
LSPM J2114+1254 A	5.3	0.14	0.71	-104.46 ± 0.31	not variable	<2.9	<0.03	0.792
LSPM J2114+1254 B	5.9	0.1		-12.70 ± 0.40				
BD -225866 Aa ^d	-0.5	0.5881	1.00	-68.97 ± 2.37	2.21 (EB)	2.21107	0.0351	0.131
BD -225866 Ab	-0.5	0.5881		58.35 ± 0.72				
BD -225866 Ba	1.0	0.49	0.90	-40.23 ± 0.53		<62	<0.3	
BD -225866 Bb	2.0	0.44		-5.41 ± 0.68				
G 67-46 A	0.3	0.6	0.82	-31.45 ± 0.78	5.00	<58.9	<0.31	≫10
G 67-46 B	1.4	0.49		24.39 ± 0.56				
GJ 4359 A	0.4	0.6	0.73	-59.78 ± 1.02	no data	<3.0	<0.04	0.017
GJ 4359 B	2.1	0.44		88.89 ± 0.33				

Table 2—Continued

Name	SpT M-(± 0.5)	Mass ^a M_{\odot}	q	RV km s^{-1}	P_{rot} ^b days	P_{orb} days	a AU	t_{sync} Gyr
GJ 4362 A	1.7	0.44	0.82	-10.32 ± 0.14	11.15	<20.8	<0.14	11.403
GJ 4362 B	3.2	0.36		60.92 ± 0.53				

^aMasses were derived from the component spectral types using data from Reid & Hawley (2005).

^bRotation periods as observed by WASP photometry. The period uncertainty is $\lesssim 0.1$ days.

^c P_{max} for 2M0008+4757 and G274-113 is 4.63 and 3.63 days, respectively.

^dObservations of this ESB4 are published in Shkolnik et al. (2008).

Table 3. Targets with detected rotation period

Name	N data Points	Date begin HJD-2450000	Date end HJD-2450000	Period ^a days	Amplitude Δmag	$\delta\chi^2/\chi_{best}^2$ ^a	Year	Note
2MASS J00080642+4757025	5381	4306.58	4451.50	4.38	0.022	0.48	2007	
LHS 6032	4118	4332.58	4460.52	4.05	0.008	0.36	2007	
G 274-113	5856	4677.52	4813.45	2.89	0.006	0.30	2008	
GJ 3129	1009	4733.52	4767.65	4.01	0.089	1.07	2008	
GJ 206	4662	4752.58	4863.47	7.59	0.013	0.89	2008-9	
2MASS J07282116+3345127	9658	4056.55	4172.50	3.57	0.028	0.69	2006	
	714	4405.58	4455.75	3.55	0.044	0.30	2007	
	602	4491.40	4554.46	3.54	0.042	1.41	2008	
2MASS J08082487+4347557	6784	4056.58	4172.50	9.70	0.005	0.29	2006	
GJ 1108 B	5616	4056.59	4172.50	3.37	0.030	2.48	2006	
	698	4056.59	4172.50	3.37	0.048	11.46	2007	
	729	4491.39	4554.42	3.40	0.027	4.38	2008	
NLTT 48838	1780	4297.45	4369.40	1.12	0.040	1.98	2007	with no systematics
BD -225866	4579	3862.58	4052.31	2.20	0.019	1.57	2006	Eclipsing
	4557	4250.53	4418.34	2.20	0.029	4.61	2007	
	5509	4622.51	4764.41	1.10	0.006	0.21	2008	period harmonic detected at $1/2 P_{orb}$, marginal
G 67-46	2555	4672.56	4767.52	5.00	0.015	1.20	2008	
GJ 4362	5068	3870.61	4054.47	11.13	0.024	1.42	2006	
	5722	4268.53	4433.44	11.16	0.026	1.10	2007	

^aThe period uncertainty is $\lesssim 0.1$ days.

^bHere we use the statistics and formalisms of Zechmeister & Kürster (2009). Their figure of merit to determine a variable signal is the improvement in χ^2 with the sinusoidal fit compared to a flat model divided by the χ^2 of the best fitting sinusoidal model. Real detections have $\delta\chi^2/\chi_{best}^2 \geq 0.28$.

Table 4. Targets with no detected rotation period

Name	N data Points	Date begin HJD-2450000	Date end HJD-2450000	$\delta\chi^2/\chi_{best}^2$	Year	Notes
NLTT 6638	11664	4677.52	4813.45	0.13	2008	VB blended in SWASP data
GJ 3240	2269	3995.58	4125.39	0.13	2007	blended with J033733.35+175114.3
NLTT 11415	2269	3995.58	4125.39	0.12	2007	blended with J033733.88+175100.6
2MASS J04244260-0647313	588	4491.32	4503.46	0.14	2008, early	
	692	4721.50	4760.75	0.01	2008, late	
CCDM J04404+3127B	949	3219.73	3278.76	0.10	2004	Eclipsing, no detectable rotational signal, blended
	2524	3995.59	4147.48	0.06	2006	
	1189	4372.59	4460.64	0.06	2007	
2MASS J08082487+4347557	1490	4419.60	4455.75	0.02	2007	
	3865	4491.39	4554.43	0.02	2008	
GJ 3630	2071	4501.52	4581.44	0.03	2008	
GJ 616.2	536	3920.38	3950.52	0.09	2006	
	10581	4189.59	4316.50	0.37	2007	1.99d period, systematics present
	8051	4553.61	4681.52	0.17	2008	
HAT 199-13890	1686	4230.59	4296.39	0.04	2007	
2MASS J21021569-3129118	11471	3862.55	4037.38	0.03	2006	
	1221	4236.50	4399.41	0.10	2007	1 day period
CCDM J2114+1254	8715	3128.66	3278.56	0.04	2004	
	7953	3908.55	4023.48	0.03	2006	

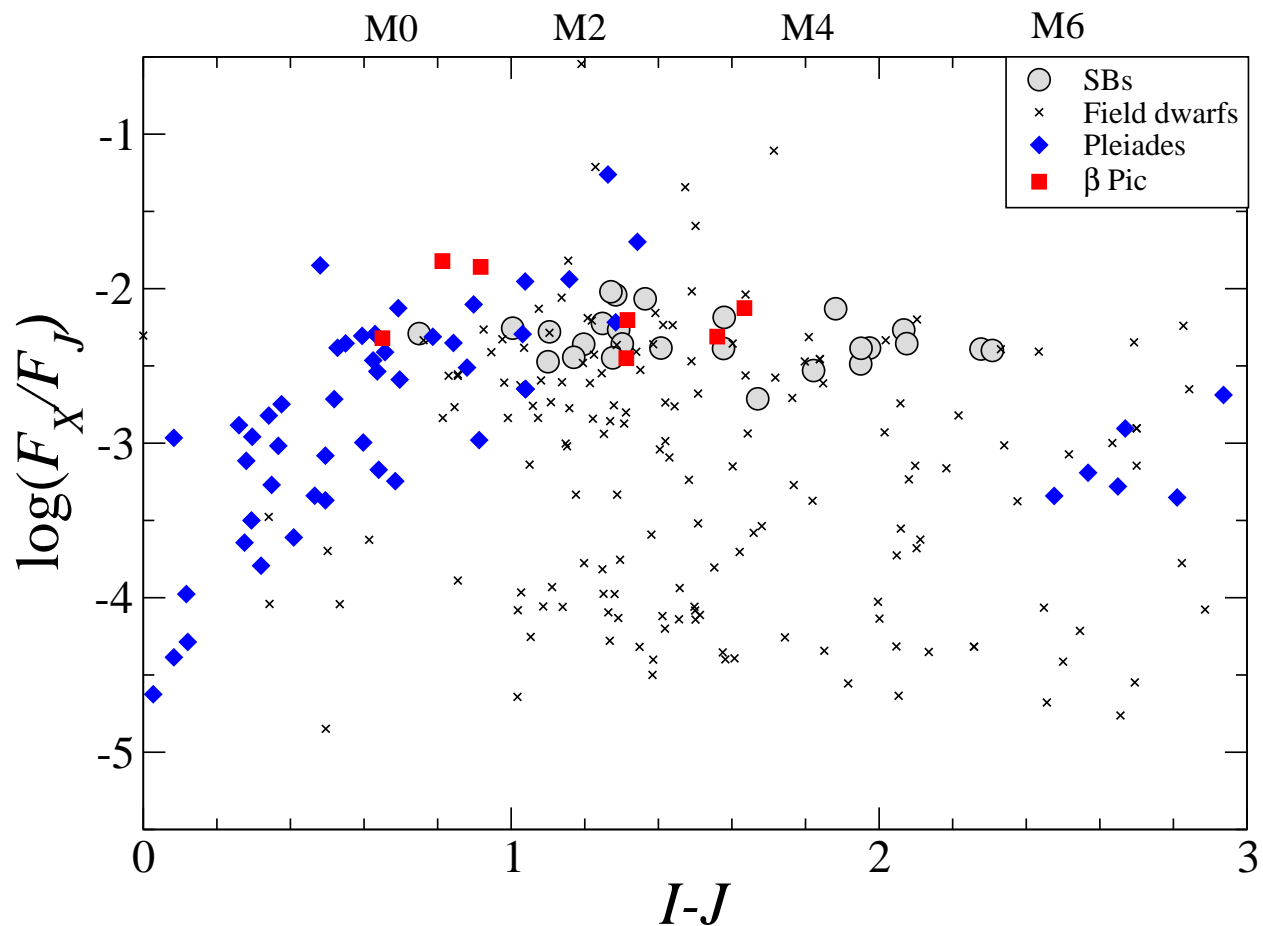


Fig. 1.— The fractional X-ray luminosity as a function of $I - J$ for our sample of SBs compared with seven members of the β Pic young moving group at 12 Myr (Torres et al. 2006), Pleiades members at 120 Myr (Micela et al. 1998), field stars (Hünsch et al. 1999).

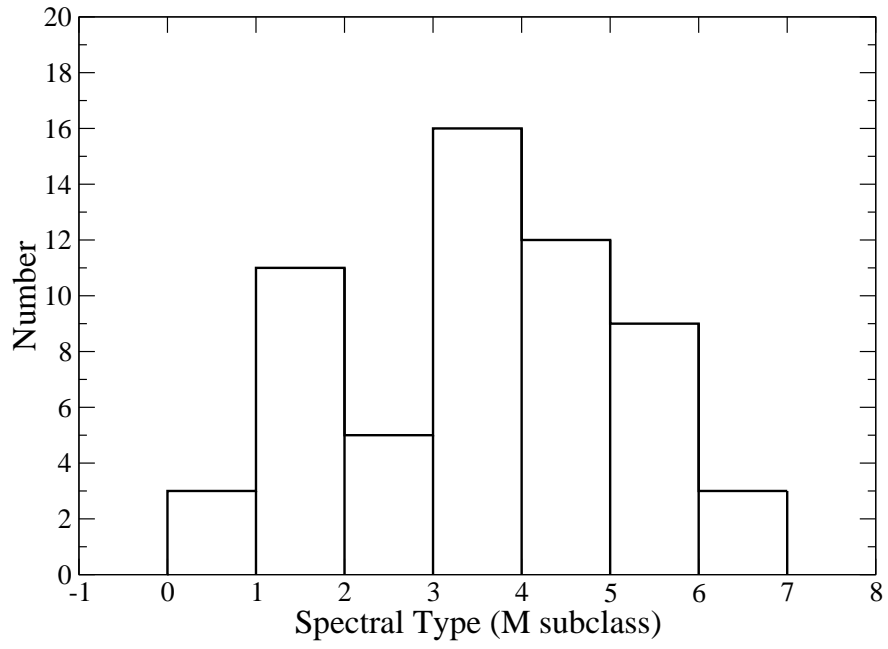


Fig. 2.— Histogram of the spectral types of the component stars.

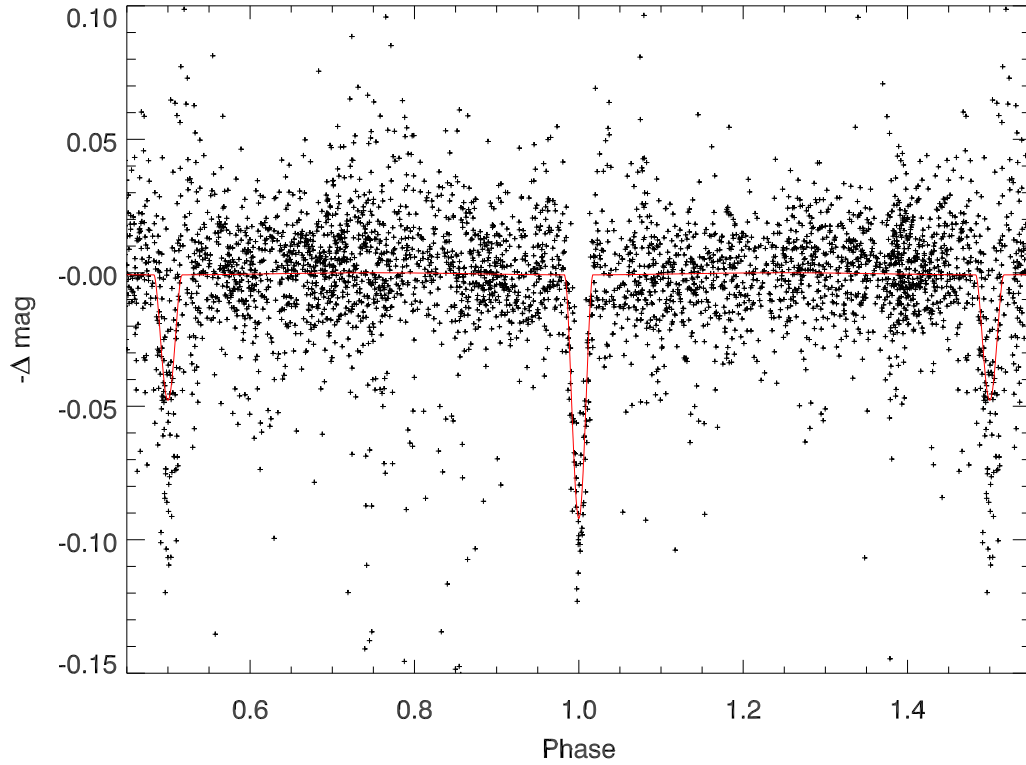


Fig. 3.— WASP light curve of CCDM J04404+3127B phase-folded with the ephemeris $(2454129.2969 \pm 0.0007) + (2.048135 \pm 0.000003)E$. Over-plotted (red line) is the best fitting EBOP model. There is no detectable rotational variability in the light curve. We also note that the eclipsing binary, CCDM J04404+3127B, is blended with CCDM J04404+3127A in the WASP photometry causing the eclipse depths to appear shallower than they should.

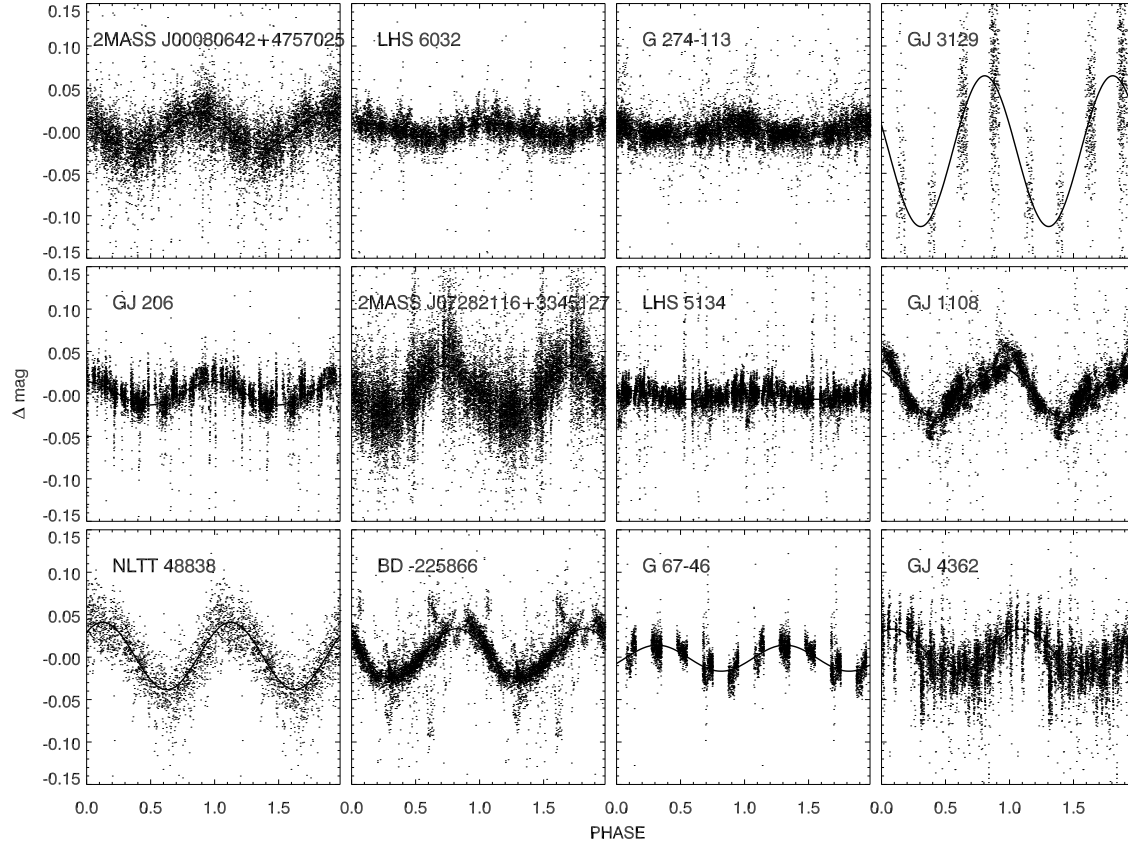


Fig. 4.— Phase-folded WASP light curves of the 12 M dwarf SBs for which rotation periods are detected. The rotation period listed in Table 3 is used to convert HJDs to phase values. The best fitting model sine curve for each target is over plotted on the phase-folded data. Note: if more than one season of WASP data exists, the one with the strongest signal is shown.

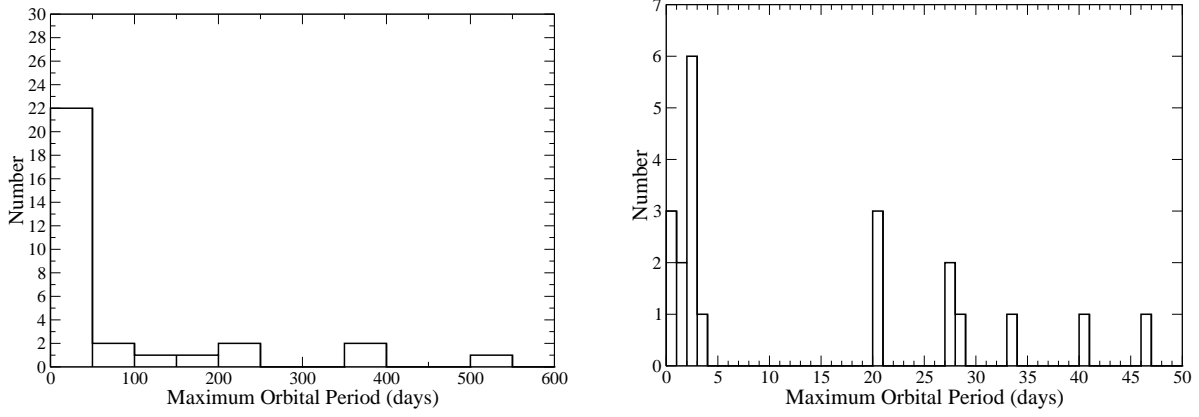


Fig. 5.— *Left:* Histogram of orbital periods consisting of P_{max} and P_{orb} if available. *Right:* An expanded histogram of the tightest orbits.

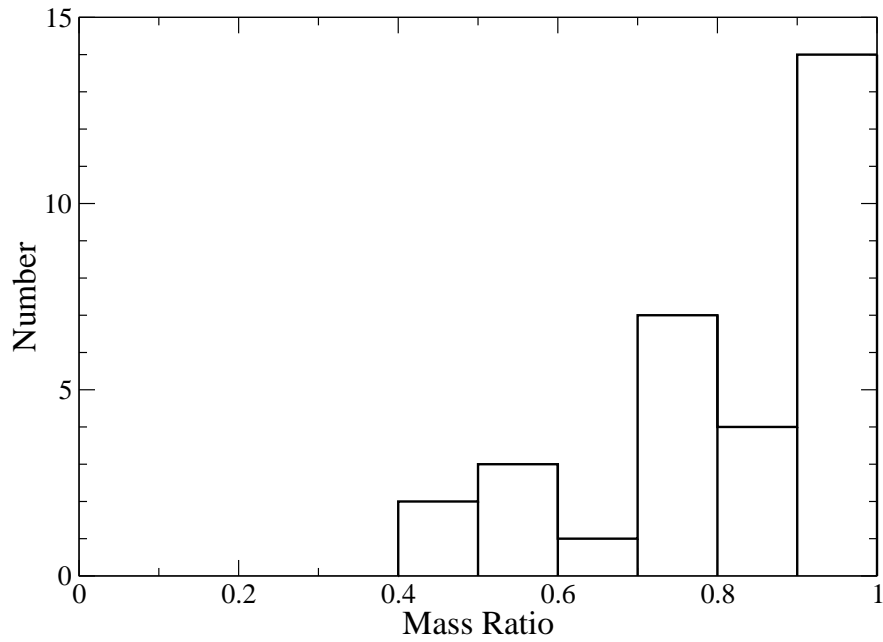


Fig. 6.— Histogram of SB mass ratios.